0013-7227/07/$15.00/0
Printed in U.S.A.

Endocrinology 148(8):3773–3780
Copyright © 2007 by The Endocrine Society
doi: 10.1210/en.2006-1691

Mineralocorticoid Receptor Blockade Attenuates Chronic Overexpression of the Renin-Angiotensin-Aldosterone System Stimulation of Reduced Nicotinamide Adenine Dinucleotide Phosphate Oxidase and Cardiac Remodeling

Sameer Stas, Adam Whaley-Connell, Javad Habibi, Lama Appesh, Melvin R. Hayden, Poorna R. Karuparthi, Mahnaz Qazi, E. Matthew Morris, Shawna A. Cooper, C. Daniel Link, Craig Stump, Meredith Hay, Carlos Ferrario, and James R. Sowers

Divisions of Endocrinology (S.S., M.R.H., J.R.S.) and Nephrology (A.W.-C.), Diabetes and Cardiovascular Lab (S.S., A.W.-C., J.H., L.A., M.Q., E.M.M., S.A.C., J.R.S.), University of Missouri School of Medicine (S.S., A.W.-C., J.H., L.A., M.R.H., P.R.K., M.Q., E.M.M., S.A.C., J.R.S.), Columbia, Missouri 65212; Harry S. Truman Veterans Administration Medical Center (A.W.-C., J.H., L.A., J.R.S.), Columbia, Missouri 65201; Department of Medicine (C.S., C.D.L), The University of Arizona, Tucson, Arizona 85721; University of Iowa (M.H.), Iowa City, Iowa 52242; and Wake Forest University School of Medicine (C.F.), Winston-Salem, North Carolina 27157

The renin-angiotensin-aldosterone system contributes to cardiac remodeling, hypertrophy, and left ventricular dysfunction. Angiotensin II and aldosterone (corticosterone in rodents) together generate reactive oxygen species (ROS) via reduced nicotinamide adenine dinucleotide phosphate (NADPH) oxidase, which likely facilitate this hypertrophy and remodeling. This investigation sought to determine whether cardiac oxidative stress and cellular remodeling could be attenuated by *in vivo* mineralocorticoid receptor (MR) blockade in a rodent model of the chronically elevated tissue renin-angiotensin-aldosterone system, the transgenic TG (mRen2) 27 rat (Ren2). The Ren2 overexpresses the mouse renin transgene with resultant hypertension, insulin resistance, proteinuria, and cardiovascular damage. Young (6- to 7-wk-old) male Ren2 and age-matched Sprague-Dawley rats were treated with spironolactone or placebo for 3 wk. Heart tissue ROS, immunohistochemical analysis of 3-nitrotyrosine, and NADPH oxidase (NOX) subunits (gp91^{phox} recently renamed NOX2, p22^{phox}, Rac1, NOX1, and NOX4) were measured. Structural changes were assessed with cine-magnetic resonance imaging, transmission electron microscopy, and light microscopy. Significant increases in Ren2 septal wall thickness (cine-magnetic resonance imaging) were accompanied by perivascular fibrosis, increased mitochondria, and other ultrastructural changes visible by light microscopy and transmission electron microscopy. Although there was no significant reduction in systolic blood pressure, significant improvements were seen with MR blockade on ROS formation and NOX subunits (each $P < 0.05$). Collectively, these data suggest that MR blockade, independent of systolic blood pressure reduction, improves cardiac oxidative stress-induced structural and functional changes, which are driven, in part, by angiotensin type 1 receptor-mediated increases in NOX. (*Endocrinology* 148: 3773–3780, 2007)

THERE IS ACCUMULATING evidence that mineralocorticoids play an important role in adverse cardiac remodeling associated with cardiac fibrosis (1–3) and perivascular inflammation (4–6). The initial pathogenic event in mineralocorticoid-induced myocardial damage is inflammatory injury of blood vessels leading to reactive fibrosis (1–6). Both cardiomyocytes and cardiac fibroblasts express mineralocorticoid receptors (MRs) with high affinity for aldosterone and corticosterone (7–9). Effects of aldosterone or corticosterone in the heart appear to involve an interaction with the renin-angiotensin-aldosterone system (RAAS), as well as direct effects of mineralocorticoid to increase cardiac fibrosis (10–18). In aldosterone and salt-treated rats, angiotensin type 1 receptor (AT_1R) expression and the ventricular density of the AT_1R have been observed to increase (18). Furthermore, mineralocorticoids have increased expression of the angiotensin-converting enzyme in cardiomyocytes from adult rat primary (19) and in cultured fetal rat cardiomyocytes (12). More recently, data from two laboratories suggest that MR activation may potentiate the proinflammatory/fibrotic effects of AT_1R signaling by enhancing the cardiac oxidative stress induced by angiotensin II (Ang-II) (17–20).

A number of clinical studies have suggested that blockade of MR is cardioprotective. Even at subpressor doses (25 mg daily), the MR antagonist spironolactone has reduced all cause mortality in patients with severe heart failure already

First Published Online May 10, 2007

Abbreviations: Ang-II, Angiotensin II; AT_1R, angiotensin type 1 receptor; C, control; EF, ejection fraction; ID, intercalated disc; LV, left ventricle; MR, mineralocorticoid receptor; MRI, magnetic resonance imaging; NADPH, reduced nicotinamide adenine dinucleotide phosphate; NOX, reduced nicotinamide adenine dinucleotide phosphate oxidase; RAAS, renin-angiotensin-aldosterone system; ROS, reactive oxygen species; SBP, systolic blood pressure; SD, Sprague-Dawley; SP, spironolactone-treated; TEM, transmission electron microscopy; VVG, Verhoeff-van Gieson.

***Endocrinology* is published monthly by The Endocrine Society (http://www.endo-society.org), the foremost professional society serving the endocrine community.**

receiving standard therapy, including an angiotensin-converting enzyme inhibitor (21). In addition, spironolactone therapy has been associated with reduced circulating levels of procollagen type III N-terminal amino peptide, a marker of collagen turnover, suggesting that MR blockade exerts beneficial antifibrotic effects in patients with heart failure (22). Animal studies have also demonstrated similar beneficial effects of MR blockade on myocardial reactive fibrosis (14–16, 23, 24) that were independent of blood pressure effects. These effects may be modulated, in part, by reduction of myocardial oxidative stress. Consistent with this notion, *in vivo* treatment with a reduced nicotinamide adenine dinucleotide phosphate (NADPH) oxidase inhibitor prevented cardiac fibrosis in aldosterone-infused rats (24). More recently, MR inhibition has reduced cardiac oxidative stress and inflammation in rodent models of chronic pressure overload (25, 26). Finally, it has been reported that spironolactone treatment partially suppressed cardiac inflammatory/fibrogenic and oxidative stress responses *in vivo* after Ang II infusion of normotensive Sprague-Dawley (SD) rats (17).

There is growing evidence that the autocrine/paracrine actions of Ang-II and mineralocorticoids are responsible for many of the adverse effects of the RAAS (1–6). Increased oxidative stress and inflammation have been observed in the kidney (27, 28) and skeletal muscle (29) of the TG(mRen2)27 rat (Ren2), which overexpresses the mouse renin transgene in these tissues. In the young Ren2 rat, zona glomerulosa production of corticosterone is significantly increased because adrenal transgenic, pro-renin production is under regulatory control of ACTH (30). Furthermore, in rats double transgenic for the human renin and angiotensin genes, MR blockade attenuated vascular injury, as well as the expression of inflammatory markers (15). These data suggest that mineralocorticoids enhance the inflammatory and fibrotic effects of Ang-II. However, the mechanisms underlying interactive actions of Ang-II and mineralocorticoids in promoting cardiac inflammation, fibrosis, and remodeling, *in vivo*, remain poorly understood. Because both Ang-II (31) and mineralocorticoids (18, 31) promote oxidative stress via NADPH oxidase (NOX) activation in cardiovascular tissues, we sought to investigate the impact of *in vivo* MR blockade with low-dose spironolactone on NOX activity, generation of reactive oxygen species (ROS), and cardiac remodeling in a model of chronic tissue RAAS overexpression, the Ren2 transgenic rat.

Materials and Methods

Animals and treatments

All animal procedures were approved by the University of Missouri animal care and use committees, and animals were housed in accordance with National Institutes of Health guidelines. Ren2 (6–7 wk of age) and age-matched SD rats were randomly assigned to untreated [Ren2-C (n = 5) and SD-C (n = 6), respectively] or spironolactone-treated [Ren2-SP (n = 6) and SD-SP (n = 4)] paradigms. Ren2 SP and SD SP animals were implanted with sc time-release, matrix-driven delivery pellets (Innovative Research of America, Sarasota, FL) containing either spironolactone (5 mg; 0.24 mg/d) or placebo for 21 d (32).

Systolic blood pressure (SBP) and body weight

Restraint conditioning was initiated on the day of initial blood pressure measurements. SBP was measured in triplicate, on separate occasions throughout the day, using the tail-cuff method (Harvard Systems, Student Oscillometric Recorder) before initiation of treatment and on d 19 or 20 before killing (27–29). Total body weight was obtained before initiation of treatment and at the time of killing.

In vivo cine-magnetic resonance imaging (MRI)

MRI scans were performed on Ren2 and SD rats pre- and posttreatment using a Varian 7T horizontal bore MRI (Varian Inc., Palo Alto, CA) with electrocardiogram gating (SA Instruments, Inc., Stony Brook, NY). Animals were anesthetized using 2–3.5% isoflurane on a nose-cone nonrebreathing system supplying continuous oxygen. A series of cine-images of the left ventricle (LV) in both long and short axis views were acquired at 12 equally spaced time points throughout the entire cardiac cycle with a frame rate of 9–13 msec. The total acquisition time of each cine-sequence was approximately 6 min with in plane spatial resolution of $156 \times 137\ \mu m^2$ (long-axis view) or $156 \times 156\ \mu m^2$ (short-axis view) and two signal averages. Heart wall thickness and left ventricular volume measurements were determined using VnmrJ (Varian, Inc., Palo Alto, CA) and ImageJ 228 (National Institutes of Health, Bethesda, MD). LV ejection fractions (EFs) were calculated using a modified ellipsoid equation (33). Intraventricular wall thickness was measured at five positions and averaged using a single transverse axial image captured at 0-msec delay after the R wave.

Transmission electron microscopy (TEM) methods

Heart tissue was thinly sliced and placed in primary electron microscopy (EM) fixative as described (27, 28). After secondary fixation, specimens were placed on a rocker overnight, embedded, and polymerized at 60 C for 24 h. There were 85-nm thin sections then stained with 5% uranyl acetate and Sato's Triple lead stain for viewing by a transmission electron microscope.

Light microscopy

Fixed paraffin sections of LV were evaluated with Verhoeff-van Gieson (VVG), which stains elastin (black), nuclei (blue black), collagen (red), and connective tissue (yellow) (28). Slides were analyzed with a Nikon50i microscope (Nikon Corp., Tokyo, Japan), and 4, 10, and 40× images were captured with a CoolSNAP$_{cf}$ camera (Photometrics, Roper Scientific, Inc., Tucson, AZ). Morphometric analysis was performed using MetaVue software (Boyce Scientific Inc., Gary Summit, MO). In each image, the perimeters of the adventitia, media, and lumen of 15–20 arteries were traced, and the percentage area was then calculated by subtracting the combined areas for media and lumen from the total area, and then dividing by the total area.

Measurement of heart tissue oxidative stress

The formation of ROS in LV sections was evaluated by chemiluminescence and further by immunostaining for 3-nitrotyrosine content, a marker of peroxynitrite formation. Tissue sections were homogenized in sucrose buffer [250 mM sucrose, 0.5 mM EDTA, 50 mM HEPES, and protease inhibitor tablet (pH 7.5)] using a glass/glass homogenizer. Homogenates were centrifuged 1500 rcf × 10 min at 4 C. Supernatants (whole homogenate) were then removed and placed on ice. Whole homogenate (100 μl) was added to 1.4-ml 50 mM phosphate (KH_2PO_4) buffer [150 mM sucrose, 1 mM EGTA, 5 μM lucigenin, and 100 μM NADPH (pH 7.0)] in dark-adapt counting vials. After dark adaptation for 1 h, samples were counted every 30 sec for 10 min on a scintillation counter, and the last 5 min were averaged. Samples were then normalized to total protein in the whole homogenate. Values are expressed as counts per minute per milligram (cpm/mg) of protein.

To assess myocardial 3-nitrotyrosine content, two LV sections per animal were deparaffinized, rehydrated, and epitopes were retrieved in citrate buffer (28). Endogenous peroxidases were quenched with 3% H_2O_2, and nonspecific binding sites were blocked with avidin, biotin, and protein block (Dako, Carpinteria, CA). The sections were then incubated with 1:200 primary rabbit polyclonal anti-Nitrotyrosine antibody (Chemicon, Temecula, CA). Sections were then washed and incubated with secondary antibodies, linked, and labeled with Streptavidin (Dako) for 30 min each. After several rinses with distilled

water, diaminobenzidine was applied for 10 min. The sections were again rinsed with distilled water, stained with hematoxylin for 1 min, rehydrated, and mounted with a permanent media. The slides were evaluated under a bright-field microscope (Nikon 50i), and eight to 10 images at ×40 were captured with a CoolSNAP$_{cf}$ camera. All computer and microscope settings were kept constant throughout the experiment. Images were analyzed blinded, and the signal intensities were measured with MetaVue.

Immunofluorescent studies

Harvested LV was immersed and fixed in 3% paraformaldehyde (27–29). After fixation, tissues were placed in histological cassettes, and dehydrated with ethanol, infiltrated with low-melting (50 C) paraplast, and embedded in high-melting (56 C) paraplast. Blocks were sectioned, deparaffinized in CitriSolv (Thermo Fisher Scientific, Waltham, MA), and rehydrated in ethanol and HEPES wash buffer. Seven sections of LV of each animal were used for analysis. The first section was washed (3 × 15 min) with HEPES wash buffer and then mounted with Mowiol (first control level) (PolySciences, Inc., Warrington, PA). The second section was washed and incubated with 1:100 primary antibodies in 10-fold diluted blocking agent (second control), and the third/fourth sections were washed and kept in the blocker. Over the course of 48 h, a fifth, sixth, and seventh section was incubated with 1:100 of goat anti-gp91^{phox} (recently renamed NOX2), mouse anti-Rac1 (Upstate Cell Signaling, Millipore Corp., Billerica, MA), goat anti-p22^{phox}, rabbit anti-Nox1 (Santa Cruz Biotechnology, Santa Cruz, CA), and goat anti-Nox4 (Santa Cruz Biotechnology) antibodies, respectively, in 10-fold diluted blocker. After 24 h, the slides were washed (3 × 15 min), and a seventh section was mounted with Mowiol (third control). Other sections were incubated with 1:300 of Alexa fluor rabbit antigoat 647 (Invitrogen Corp., Carlsbad, CA) in 10-fold diluted blocker except the sixth, which was stained with 1:300 of Alexa fluor goat antimouse 647. After 4 h, the slides were washed, mounted with Mowiol, and examined using a laser confocal scanning microscope (Bio-Rad, Hercules, CA). Eight to 10Z optical images were captured from each section using a ×60 water lens of a confocal microscope. All computer and microscope settings were kept the same throughout the experiments. The resolution of each image was 1024 × 1024 pixels. Images were captured blinded, using the Laser-sharp software (Bio-Rad) and signal intensities measured by MetaVue analysis (27).

Statistical analysis

All values are expressed as mean ± SE. Statistical analyses were performed in SPSS 13.0 (SPSS, Inc., Chicago, IL) using paired or unpaired Student's *t* tests, or ANOVA with Fisher's least significant difference as appropriate.

Results

SBP and cine-MRI

At initiation of treatment (6–7 wk of age), SBPs were higher in Ren2-C compared with SD-Cs ($P < 0.05$) (Table 1). At the end of the treatment period (9–10 wk of age), there was no difference in SBP between Ren2-C and Ren2-SP ($P > 0.05$). *In vivo* cine-MRI was used to measure septal wall thickness (Fig. 1A) and systolic EF (Fig. 1B) before initiation and at the end of treatment. At baseline, there was no significant difference in septal wall thickness among the groups. At 8–9 wk of age, septal wall thickness was significantly increased in the Ren2-C (1.9 ± 0.06 mm; δ 0.64 ± 0.08) compared with SD-C (1.65 ± 0.04 mm; δ 0.34 ± 0.09) ($P < 0.05$), an effect that was attenuated by spironolactone treatment (1.78 ± 0.05 mm; δ 0.24 ± 0.07) ($P = 0.06$, $P < 0.05$). In addition, no significant differences were found with respect to systolic EF at baseline or posttreatment in the Ren2 compared with SD rats in either treatment or control groups ($P > 0.05$) (Fig. 1B).

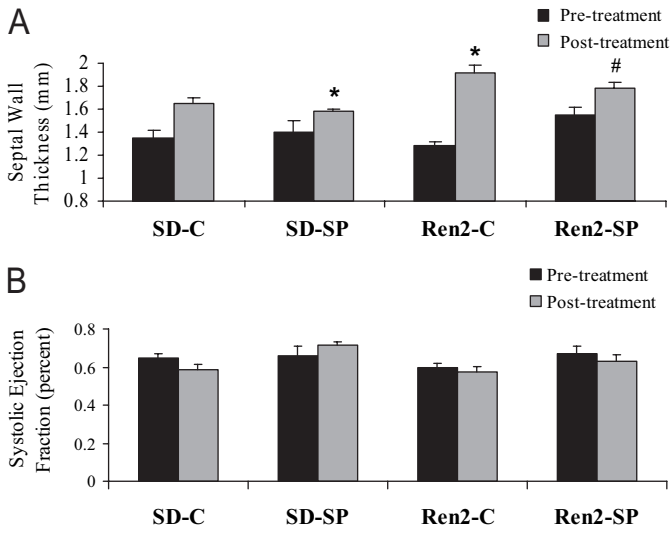

FIG. 1. Cine-MRI evaluation of cardiac remodeling. A, *In vivo* cine-MRI measures of heart septal wall thickness pre- and posttreatment. *, $P < 0.05$ when Ren2-Cs are compared with age-matched SD-Cs; #, $P = 0.06$ when Ren2-SPs are compared with age-matched Ren2-C. B, Systolic EF pre- and posttreatment. No significant differences were seen among groups ($P > 0.05$).

Heart tissue oxidative stress

ROS formation was increased in Ren2-C (4266 ± 1191 cpm/mg; $P < 0.05$), an effect that was abrogated with spironolactone (3207 ± 446 cpm/mg; $P < 0.05$) (Fig. 2A). There were similar increases observed with immunostaining of nitrotyrosine, a measure of peroxynitrite ($ONOO^-$) formation, in the Ren2-C (62.8 ± 2.6 average gray-scale intensities) when compared with SD-C (41.6 ± 9.7 average gray-scale intensities; $P < 0.05$) that was again improved in the Ren2-SP (41.1 ± 1.9 average gray-scale intensities; $P < 0.05$) (Fig. 2, B and C).

NOX subunits

Evaluation of NOX subunits NOX2, Rac1, and p22^{phox}, as well as NOX1 and NOX4 via immunohistochemistry re-

TABLE 1. Experimental parameters

	SD-C	SD-SP	Ren2-C	Ren2-SP
Weight				
Initial (g)	102.5 ± 19.4	142.8 ± 16.0	108.8 ± 2.1	137.8 ± 12.7
Final (g)	256.2 ± 9.7	254.0 ± 6.9	254.8 ± 7.3	266.6 ± 10.5
SBP				
Initial (mm Hg)	126.2 ± 3.7	142.7 ± 4.7	144.6 ± 1.7[a]	153.8 ± 6.4[a]
Final (mm Hg)	139.5 ± 3.8	143.3 ± 5.1	189.6 ± 3.0[a]	199.4 ± 7.5

[a] $P < 0.05$ when age-matched Ren2-Cs or Ren2-SPs are compared with SD-Cs.

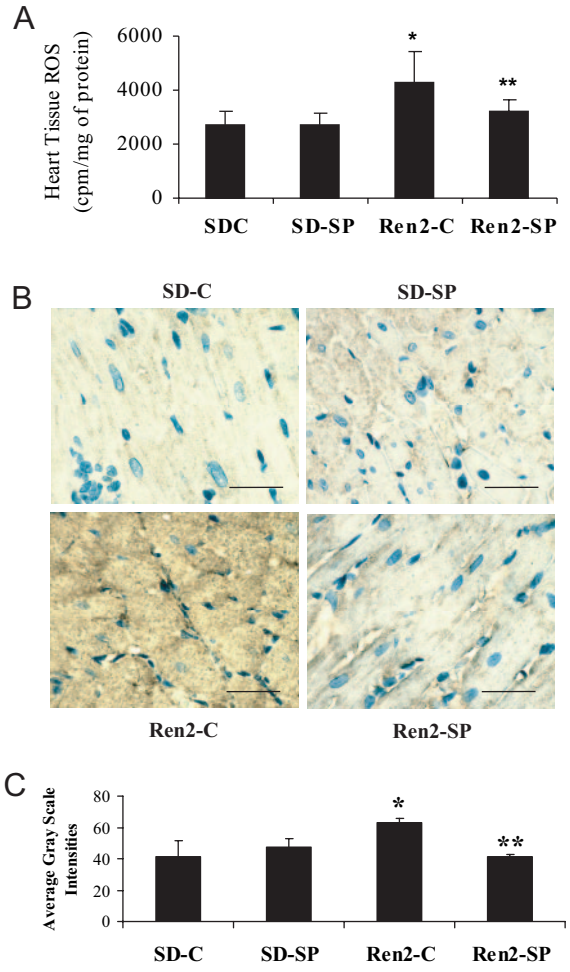

FIG. 2. Spironolactone decreases cardiac oxidative stress markers in Ren2 rats. A, Heart tissue formation of ROS in the Ren2. B, Representative sections of LV stained for nitrotyrosine, a marker of peroxynitrite ($ONOO^-$) formation. All *scale bars* in *black* are 50 μm. Magnification, ×40. C, Gray-scale intensity measures of the nitrotyrosine immunostaining. *, $P < 0.05$ when Ren2-Cs are compared with SD-Cs; **, $P < 0.05$ when Ren2-SPs are compared with Ren2-Cs.

vealed increases in NOX2, Rac1, and $p22^{phox}$ in the Ren2-C (40.2 ± 7.2, 38.8 ± 6.4, and 23.6 ± 2.9 average gray-scale intensities, respectively) when compared with SDC (26.7 ± 1.0, 21.7 ± 1.2, and 16.5 ± 0.8 average gray-scale intensities, respectively; $P < 0.05$) (Fig. 3, A and B). Although the NOX1 and four subunits in the Ren2-C were not elevated compared with the SD-C ($P > 0.05$), there were significant reductions in each subunit in the Ren2-SP (NOX2, 17.9 ± 1.8 average gray-scale intensities; Rac1, 14.7 ± 1.0 average gray-scale intensities; ($p22^{phox}$, 16.2 ± 1.5 average gray-scale intensities; NOX1, 34.8 ± 1.8 average gray-scale intensities; and NOX4, 23.8 ± 1.8 average gray-scale intensities) when compared with Ren2-C (each $P < 0.05$).

Light microscopy and TEM

Perivascular fibrosis, as represented by percent area of adventitia presenting fibrosis on VVG staining, was increased in the Ren2-C (70 ± 2.9%) compared with the SD-C (57 ± 3.7%) ($P < 0.05$) that was improved in the Ren2-SP (57.8 ± 4.3%) compared with the Ren2-C ($P < 0.05$) (Fig. 4, A and B). Interestingly, there were no significant changes in the area of the media or lumen in the groups ($P > 0.05$). Fibrosis emanated from the perivascular area to the interstitium of the endomysium between cardiomyocytes. Cardiomyocytes were also elongated in the Ren2-C compared with SD.

TEM images (Figs. 5 and 6) of the Ren2-C heart demonstrate striking changes in the mitochondria, intercalated discs (IDs), and Z-lines. There were increased numbers of mitochondria in the Ren2-C compared with the SD-C, and thickening of the Z-lines, as well as a prominent appearance of ID duplication in the Ren2-C compared with the SD-C (Fig. 5). Thickening (duplication) of the ID may reflect an increasing number of convolutions to lengthen this structure and increase its strength. Treated animals, Ren2-SP, displayed a substantial reduction in the development of these adaptive remodeling changes of the ID.

Discussion

Data from this investigation indicate that MR blockade with treatment of subpressor dose spironolactone for 3 wk reduced the cardiac remodeling and oxidative stress typically present in the Ren2 rodent model of tissue RAAS overexpression. A similar observation of cardiac protection without blood pressure lowering has been reported in other hypertensive rodent models (14–16, 23, 24, 34–36). This myocardial protective effect was associated with reduced NOX subunit expression and reduced 3-nitrotyrosine levels, as have been observed in several different rodent models (5, 17, 24–26).

Cardiac imaging with cine-MRI technology demonstrated increased septal wall thickness in the Ren2 heart that was abrogated by MR blockade. Despite the increased septal wall thickness, there was no abnormality of systolic function in Ren2 rats at the early age at which they were studied.

Heart failure and hypertension have each been linked to enhanced oxidative stress, in part, through activation of both systemic and tissue RAAS (5, 30, 31). Oxidative stress, in turn, is generally believed to be responsible for the proinflammatory/profibrogenic changes in the myocardium (5, 31). In this study, 8- to 10-wk-old Ren2 rats were observed to have coronary perivascular fibrosis and adventitial expansion in concert with increases in 3-nitrotyrosine staining in the perivascular region. Indeed, NOX catalyzes a one-electron reduction of molecular oxygen to superoxide (O_2^-), which can react to form short-lived peroxynitrite ($ONOO^-$), which is converted to stable 3-nitrotysrosine (31, 37). The heart has a very limited endogenous antioxidant capacity as contributed by both enzymatic and nonenzymatic-free radical scavengers and antioxidants (31, 35, 37). This characteristic renders the myocardium more susceptible than other tissues to oxidative stress with associated structural and functional abnormalities (31, 37).

Legato *et al.* (38), using TEM, described several qualitative changes in the pressure overloaded myocardium, but little follow-up work has been conducted. In that early report, they noted thickened Z-lines of the sarcomere, smaller and more numerous mitochondria, and what they describe as doubling

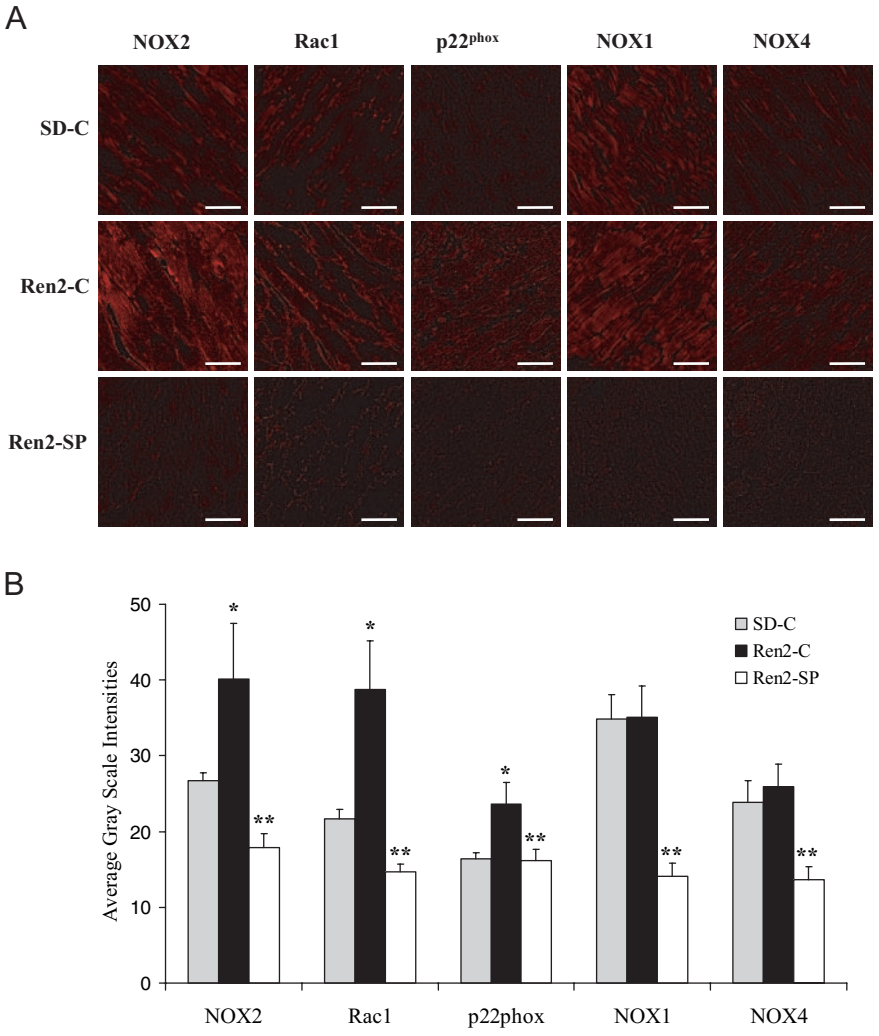

FIG. 3. Spironolactone diminishes cardiac NOX subunit expression. A, Representative images of left ventricular sections immunostained for NOX subunits NOX2, Rac1, p22^{phox}, NOX1, and NOX4. All *scale bars* in *white* are 50 μm. B, Gray-scale intensity measures of NOX subunit expression. *, $P < 0.05$ when Ren2-Cs are compared with SD-Cs; **, $P < 0.05$ when Ren2-SPs are compared with Ren2-Cs.

of the IDs. In our investigation, the untreated 8- to 10-wk-old hypertensive Ren2 had the following TEM abnormalities: thickened Z-lines; doubling or duplication of the IDs; and more plentiful, smaller interdigitating mitochondria. The duplication of IDs has been proposed to represent increased convolutions, allowing more physical contact and strength-

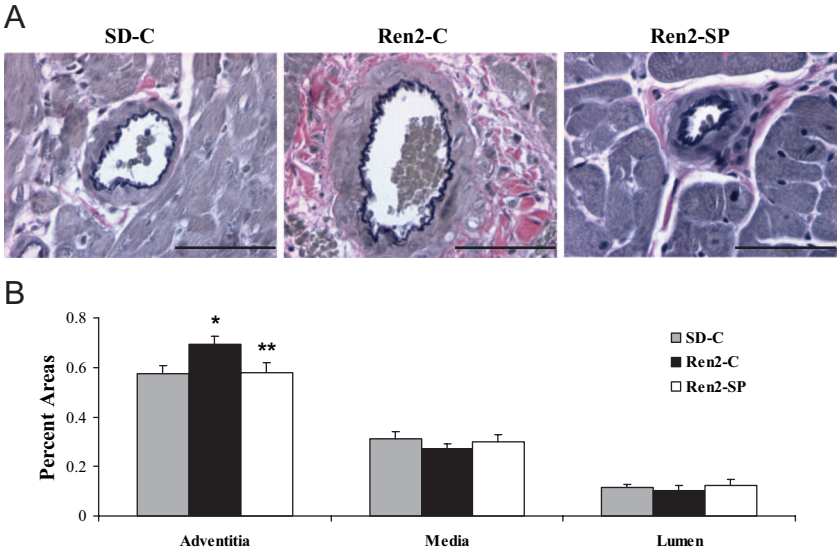

FIG. 4. Spironolactone attenuates perivascular fibrosis visible by light microscopy in Ren2 rats. A, VVG-stained sections of LV. VVG is specific for fibrosis and stains elastin (*black*), nuclei (*blue black*), collagen (*red*), and connective tissue (*yellow*). All *scale bars* in *black* are 50 μm. B, Average calculated values of percentage area of adventitia, media, and the lumen of the intramural arteries in the heart. *, $P < 0.05$ when Ren2-Cs are compared with SD-Cs; **, $P < 0.05$ when Ren2-SPs are compared with Ren2-Cs.

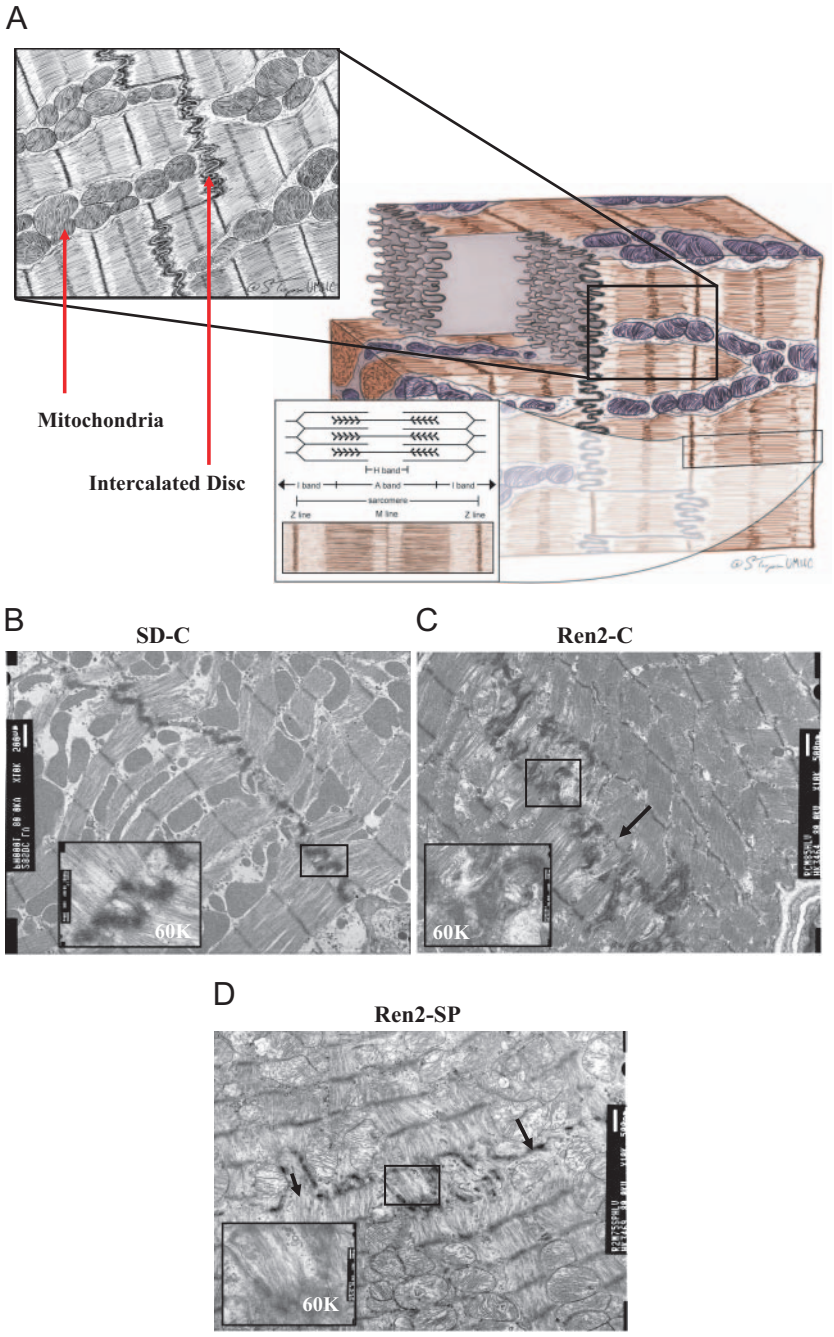

FIG. 5. Spironolactone improves ultrastructural remodeling of the ID visible by TEM in Ren2 rats. A, Normal cardiac ultrastructure with mitochondria and IDs as observed on TEM (*inset upper left*) and a sarcomere (*lower inset*) with Z lines and the I and A bands. B, Representative normal ID from the SD-C at ×10,000 magnification with a ×60,000 *inset* compared with representative remodeled ID from the Ren2-C at ×10,000 magnification. C, Duplication of the IDs noted in the Ren2-C described by others (39). The *inset* further reveals increased convolutions of the ID at ×60,000 magnification. D, Representative ID from the Ren2-SP model at ×10,000 magnification. The ID of the Ren2-SP more closely resembles the healthy SD-C in both the ×10,000 and ×60,000 *insets*.

ening of the ID in pressure overload conditions (38). Treatment with low-dose spironolactone lessened this duplication and decreased the number of interdigitating mitochondria. This represents the first TEM examination of Ren2 hearts, as well as the first study to examine the impact of MR blockade therapy. The noted changes occurred in concert with light microscopy observations of perivascular inflammatory/fibrogenic alterations and increased perivascular nitrotyrosine staining. Thus, our data suggest that Ang-II and mineralocorticoid interact to increase induction of oxidative stress, which leads to myocardial inflammation and fibrosis with accompanying alterations in IDs and mitochondria that likely reflect redox-mediated alterations.

The MR-mediated cardiac effects may have been produced by either glucocorticoid or mineralocorticoid stimulation because the MR in the heart is also activated by endogenous glucocorticoids, including cortisol in humans and corticosterone in rodents (39, 40). These two glucocorticoids express the same affinity for the MR as aldosterone (39). Furthermore, corticosterone is present in the blood at concentrations 2 orders of magnitude greater than aldosterone (39, 40). Myocardial expression of the 11 β-hydroxysteroid dehydrogenase (oxidase form) in the heart (8) gives glucocorticoids the same or greater degree of access as mineralocorticoids to the MR in the heart (8, 39). A phagocyte-type NOX is expressed in the heart and is a major source of ROS during the devel-

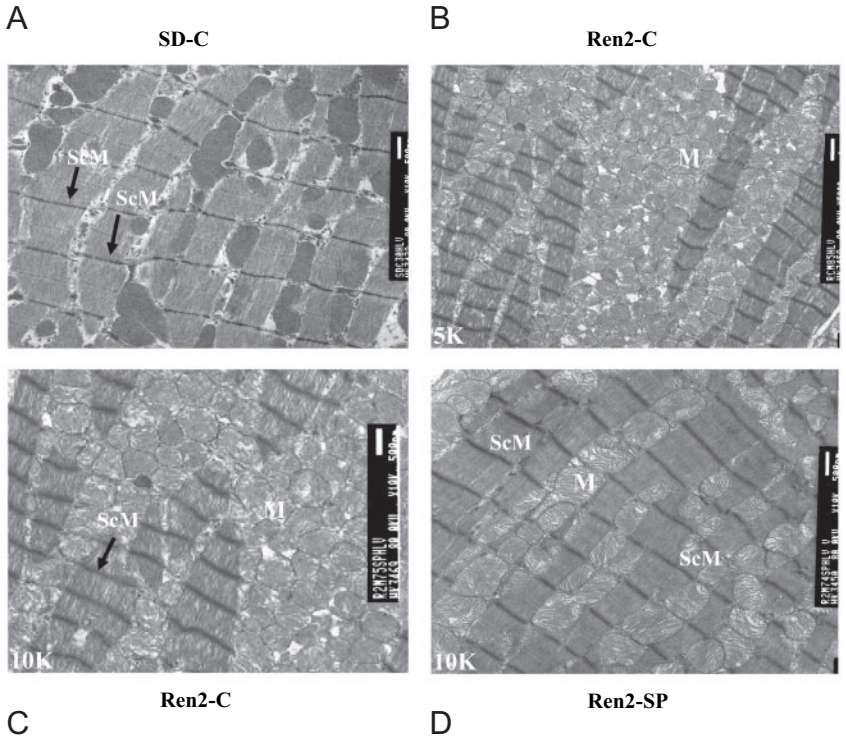

FIG. 6. Spironolactone improves ultrastructural remodeling visible TEM in Ren2 rats. A, Representative image from the SD-C demonstrating a line of sarcolemmal mitochondria (M) just beneath the sarcomeres (ScM; the distance between two Z lines) of the myocardium at ×10,000 magnification. B, Representative remodeled mitochondria in the Ren2-C. This image represents a marked increase of interdigitating mitochondria at ×5,000 magnification. C, The same image as in panel B at ×10,000 magnification to compare to SD-C and Ren2-SP in (D). D, A representative ×10,000 image from the Ren2-SP at ×10,000 magnification. Note the improved appearance of the sarcolemmal mitochondria with the spironolactone treatment. The mitochondria in this model now possess an appearance more similar to the SD-C (A) with a monolayer of mitochondria beneath the sarcomeres.

opment of pressure overload cardiac hypertrophy (40), as exists in the Ren2 rat. Aldosterone-induced MR activation results in stimulation of vascular NOX (20, 30). Furthermore, glucocorticoid-MR complexes are activated as a result of ROS generation (40, 41). Thus, the RAAS and ROS pathways can interact to result in multiplicative injury to the heart. Treatment with low, nonblood pressure lowering doses of spironolactone appears to interrupt this process by suppression of MR signaling.

At least five subunits of the NOX have been observed previously in the heart (18, 39, 42). The myocardium of the Ren2 heart manifested increased NOX2, $gp22^{phox}$, and Rac1 subunits. In concert with decreases in NOX subunit expression, ROS formation, and 3-nitrotyrosine staining after low-dose spironolactone treatment, there was decreased activated membrane Rac1. Given the seminal role of Rac1 translocation to the membrane in activation of the NADPH complex, the effect of treatment to decrease membrane translocation appears to be an important underlying mechanism for the cardioprotective effects of MR blockade. Reduction of cardiac NOX2 by MR blockade is a novel finding of this investigation. The NOX2 is the catalytic subunit and the primary membrane component to which the $p40^{phox}$, $p47^{phox}$, and $p67^{phox}$ complex binds via Rac1 activation (30, 31). Elevation of the $p40^{phox}$ subunit in the Ren2 transgenic model of tissue RAAS overexpression, and the subsequent reduction with MR blockade, is another novel observation. Although the precise role of $p40^{phox}$ in the cardiac redox state is not well understood, there is evidence that it acts as a bridge between $p47^{phox}$ and $p67^{phox}$ to assemble the NOX membrane complex (43). $p40^{phox}$ may be derived from fibroblasts on macrophages that infiltrated the myocardium (44). This is consistent with our observations of increased perivascular fibrosis, increased macrophage infiltration, and increased 3-nitrotyrosine staining in the perivascular region, changes that were substantially ameliorated by low-dose MR blockade.

Collectively, these data suggest that MR activation potentiates the proinflammatory/fibrotic effects of Ang-II by enhancing cardiac NOX-mediated oxidative stress induced by tissue RAAS activation. Furthermore, MR blockade at subpressor doses, *i.e.* independent of SBP reductions, ameliorate cardiac oxidative stress and subcellular remodeling.

Acknowledgments

We thank the Veterans Administration Biomolecular Imaging Center at the Harry S. Truman Veterans Administration Hospital and the University of Missouri-Columbia for providing their support. The authors also thank the Electron Microscope Core Facility for its help and preparation of transmission electron micrographs. Special thanks go to Suzanne Clark for her technical assistance in completion of the studies and Allison Farris for help in preparation of this manuscript.

Received December 18, 2006. Accepted April 27, 2007.

Address all correspondence and requests for reprints to: James R. Sowers, M.D., F.A.C.E., F.A.C.P., F.A.H.A., Professor of Medicine, Physiology and Pharmacology, University of Missouri-Columbia, Health Sciences Center, MA410, DC043.00, Columbia, Missouri 65212. E-mail: sowersj@health.missouri.edu.

This research was supported by National Institutes of Health (NIH) Grants R01 HL73101-01A1 (to J.R.S.) and P01 HL-51952 (to C.F.), the Veterans Affairs Merit System (0018) (to J.R.S.), and Advanced Research Career Development (to C.S.). Male transgenic Ren2 rats and male Sprague-Dawley controls were kindly provided by C.F. through the Transgenic Core Facility supported in part by NIH Grant HL-51952.

Disclosure Summary: The authors have nothing to disclose.

References

1. **Brilla CG, Zhou G, Matsubara L, Weber KT** 1994 Collagen metabolism in cultured adult rat cardiac fibroblasts: response to angiotensin II and aldosterone. J Mol Cell Cardiol 26:809–820
2. **Funder J** 2001 Mineralocorticoids and cardiac fibrosis: the decade in review. Clin Exp Pharmacol Physiol 28:1002–1006
3. **Rossi GP, Di Bello V, Ganzaroli C, Sacchetto A, Cesari M, Bertini A, Giorgi D, Scognamiglio R, Mariani M, Pessina AC** 2002 Excess aldosterone is associated with alterations of myocardial texture in primary aldosteronism. Hypertension 40:23–27
4. **Rocha R, Rudolph AE, Frierdich GE, Nachowiak DA, Kekec BK, Blomme EA, McMahon EG, Delyani JA** 2005 Aldosterone induces a vascular inflammatory phenotype in the rat heart. Am J Physiol Heart Circ Physiol 283: H1802–H1810
5. **Sun Y, Zhang J, Lu L, Chen SS, Quinn MT, Weber KT** 2002 Aldosterone-induced inflammation in the rat heart: role of oxidative stress. Am J Pathol 161:1773–1781
6. **Funder JW** 2006 Mineralocorticoid receptors and cardiovascular damage: it's not just aldosterone. Hypertension 47:634–635
7. **Lombes M, Oblin ME, Gasc JM, Baulieu EE, Farman N, Bonvalet JP** 1992 Immunohistochemical and biochemical evidence for a cardiovascular mineralocorticoid receptor. Circ Res 71:503–510
8. **Sheppard KE, Autelitano DJ** 2002 11β-hydroxysteroid dehydrogenase 1 transforms 11-dehydrocorticosterone into transcriptionally active glucocorticoid in neonatal rat heart. Endocrinology 143:198–204
9. **Qin W, Rudolph AE, Bond BR, Rocha R, Blomme EA, Goellner JJ, Funder JW, McMahon EG** 2003 Transgenic model of aldosterone-driven cardiac hypertrophy and heart failure. Circ Res 93:69–76
10. **Rocha R, Stier Jr CT, Kifor I, Ochoa-Maya MR, Rennke HG, Williams H, Adler GK** 2000 Aldosterone: a mediator of myocardial necrosis and renal arteriopathy. Endocrinology 141:3871–3878
11. **Robert V, Heymes C, Sivestre JS, Sabri A, Swynghedauw B, Delcayre C** 1999 Angiotensin AT1 receptor subtype as a cardiac target of aldosterone. Hypertension 33:981–986
12. **Harada E, Yoshimura M, Yasue H, Nakagawa O, Nakagawa M, Harada M, Mizuno Y, Nakayama M, Shimasaki Y, Ito T, Nakamura S, Kuwahara K, Saito Y, Nakao K, Ogawa H** 2001 Aldosterone induces angiotensin-converting-enzyme gene expression in cultured neonatal rat cardiocytes. Circulation 104:137–139
13. **De Angelis N, Fiordaliso F, Latini R, Calvillo L, Funicello M, Gobbi M, Mennini T, Masson S** 2002 Appraisal of the role of angiotensin II and aldosterone in ventricular myocyte apoptosis in adult normotensive rat. J Mol Cell Cardiol 34:1655–1665
14. **Rocha R, Martin-Berger CL, Yang P, Scherrer R, Delyani J, McMahon E** 2002 Selective aldosterone blockade prevents angiotensin II/salt-induced vascular inflammation in the rat heart. Endocrinology 143:4828–4836
15. **Fiebeler A, Schmidt F, Muller DN, Park JK, Dechend R, Bieringer M, Shagdarsuren E, Breu V, Haller H, Luft FC** 2001 Mineralocorticoid receptor affects AP-1 and nuclear factor-κB activation in angiotensin II-induced cardiac injury. Hypertension 37:787–793
16. **Fraccarollo D, Galuppo P, Schmidt I, Ertl G, Bauersachs J** 2005 Additive amelioration of left ventricular remodeling and molecular alterations by combined aldosterone and angiotensin receptor blockade after myocardial infarction. Cardiovasc Res 67:97–105
17. **Zhao W, Ahokas RA, Weber KT, Sun Y** 2006 ANG II-induced cardiac molecular and cellular events: role of aldosterone. Am J Physiol Heart Circ Physiol 291:H336–H343
18. **Johar S, Cave AC, Narayanapanicker A, Grieve DJ, Shah AM** 2006 Aldosterone mediates angiotensin II-induced interstitial cardiac fibrosis via a Nox2-containing NADPH oxidase. FASEB J 20:1546–1548
19. **Sun Y, Weber KT** 1996 Angiotensin converting enzyme and myofibroblasts during tissue repair in the rat heart. J Mol Cell Cardiol 28:851–858
20. **Keidar S, Kaplan M, Pavlotzky E, Coleman R, Hayek T, Hamoud S, Aviram M** 2004 Aldosterone administration to mice stimulates macrophage NADPH oxidase and increases atherosclerosis development: a possible role for angiotensin-converting enzyme and the receptors for angiotensin II and aldosterone. Circulation 109:2213–2220
21. **Pitt B, Zannad F, Remme WJ, Cody R, Castaigne A, Perez A, Palensky J, Wittes J** 1999 The effect of spironolactone on morbidity and mortality in patients with severe heart failure. Randomized Aldactone Evaluation Study Investigators. N Engl J Med 341:709–717
22. **MacFadyen RJ, Barr CS, Struthers AD** 1997 Aldosterone blockade reduces vascular collagen turnover, improves heart rate variability and reduces early morning rise in heart rate in heart failure patients. Cardiovasc Res 35:30–34
23. **Silvestre JS, Heymes C, Oubenaissa A, Robert V, Aupetit-Faisant B, Carayon A, Swynghedauw B, Delcayre C** 1999 Activation of cardiac aldosterone production in rat myocardial infarction: effect of angiotensin II receptor blockade and role in cardiac fibrosis. Circulation 99:2694–2701
24. **Park YM, Park MY, Suh YL, Park JB** 2004 NAD(P)H oxidase inhibitor prevents blood pressure elevation and cardiovascular hypertrophy in aldosterone-infused rats. Biochem Biophys Res Commun 313:812–817
25. **Kuster GM, Kotlyar E, Rude MK, Siwik DA, Liao R, Colucci WS, Sam F** 2005 Mineralocorticoid receptor inhibition ameliorates the transition to myocardial failure and decreases oxidative stress and inflammation in mice with chronic pressure overload. Circulation 111:420–427
26. **Kobayashi N, Yoshida K, Nakano S, Ohno T, Honda T, Tsubokou Y, Matsuoka H** 2006 Cardioprotective mechanisms of eplerenone on cardiac performance and remodeling in failing rat hearts. Hypertension 47:671–679
27. **Whaley-Connell A, Chowdhury NA, Hayden MR, Stump CS, Habibi J, Wiedmeyer CE, Gallagher PE, Tallant EA, Cooper SA, Link CD, Ferrario C, Sowers JR** 2006 Oxidative stress and glomerular filtration barrier injury: role of the renin-angiotensin system in the Ren2 transgenic rat. Am J Physiol Renal Physiol 291:F1308–F1314
28. **Hayden MR, Chowdhury N, Cooper SA, Whaley-Connell A, Habibi J, Witte L, Wiedmeyer CE, Manrique CM, Lastra G, Ferrario CM, Stump CS, Sowers JR** 2007 Proximal tubule microvilli remodeling and albuminuria in the Ren2 transgenic rat. Am J Physiol Renal Physiol 292:F861–F867
29. **Blendea MC, Jacobs D, Stump CS, McFarlane SI, Ogrin C, Bahtyiar G, Stas S, Kumar P, Sha Q, Ferrario CM, Sowers JR** 2005 Abrogation of oxidative stress improves insulin sensitivity in the Ren-2 rat model of tissue angiotensin II overexpression. Am J Physiol Endocrinol Metab 288:E353–E359
30. **Sander M, Bader M, Djavidani B, Maser-Gluth C, Vecsei P, Mullins J, Ganten D, Peters J** 1992 The role of the adrenal gland in hypertensive transgenic rat TGR(mREN2)27. Endocrinology 131:807–814
31. **Byrne JA, Grieve DJ, Bendall JK, Li JM, Gove C, Lambeth JD, Cave AC, Shah AM** 2003 Contrasting roles of NADPH oxidase isoforms in pressure-overload versus angiotensin II-induced cardiac hypertrophy. Circ Res 93:802–805
32. **Brown NJ, Nakamura S, Ma L, Nakamura I, Donnert E, Freeman M, Vaughan DE, Fogo AB** 2000 Aldosterone modulates plasminogen activator inhibitor-1 and glomerulosclerosis in vivo. Kidney Int 58:1219–1227
33. **Iltis I, Kober F, Dalmasso C, Lan C, Cozzone PJ, Bernard M** 2005 In vivo assessment of myocardial blood flow in rat heart using magnetic resonance imaging: effect of anesthesia. J Magn Reson Imaging 22:242–247
34. **Rocha R, Chander PN, Khanna K, Zuckerman A, Stier Jr CT**1998 Mineralocorticoid blockade reduces vascular injury in stroke-prone hypertensive rats. Hypertension 31:451–458
35. **Mazak I, Fiebeler A, Muller DN, Park JK, Shagdarsuren E, Lindschau C, Dechend R, Viedt C, Pilz B, Haller H, Luft FC**2004 Aldosterone potentiates angiotensin II-induced signaling in vascular smooth muscle cells. Circulation 109:2792–2800
36. **Martinez DV, Rocha R, Matsumura M, Oestreicher E, Ochoa-Maya M, Roubsanthisuk W, Williams GH, Adler GK** 2002 Cardiac damage prevention by eplerenone: comparison with low sodium diet or potassium loading. Hypertension 39:614–618
37. **Privratsky JR, Wold LE, Sowers JR, Quinn MT, Ren J** 2003 AT1 blockade prevents glucose-induced cardiac dysfunction in ventricular myocytes: role of the AT1 receptor and NADPH oxidase. Hypertension 42:206–212
38. **Legato MJ, Mulieri LA, Alpert NR** 1984 The ultrastructure of myocardial hypertrophy: why does the compensated heart fail? Eur Heart J 5(Suppl F): 251–269
39. **Arriza JL, Weinberger C, Cerelli G, Glaser TM, Handelin BL, Housman DE, Evans RM** 1987 Cloning of human mineralocorticoid receptor complementary DNA: structural and functional kinship with the glucocorticoid receptor. Science 237:268–275
40. **Nagata K, Obata K, Xu J, Ichihara S, Noda A, Kimata H, Kato T, Izawa H, Murohara T, Yokota M** 2006 Mineralocorticoid receptor antagonism attenuates cardiac hypertrophy and failure in low-aldosterone hypertensive rats. Hypertension 47:656–664
41. **Frey FJ, Odermatt, Frey BM** 2004 Glucorticoid- mediated mineralocorticoid receptor activation and hypertension. Curr Opin Nephrol Hypertens 13:451–458
42. **Li JM, Gall NP, Grieve DJ, Chen M, Shah AM** 2002 Activation of NADPH oxidase during progression of cardiac hypertrophy to failure. Hypertension 40:477–484
43. **Lapouge K, Smith SJ, Groemping Y, Rittinger K** 2002 Architecture of the p40–p47-p67phox complex in the resting state of the NADPH oxidase. A central role for p67phox. J Biol Chem 277:10121–10128
44. **Keidar S, Heinrich R, Kaplan M, Aviram M** 2002 Oxidative stress increases the expression of the angiotensin-II receptor type 1 in mouse peritoneal macrophages. J Renin Angiotensin Aldosterone Syst 3:24–30

***Endocrinology* is published monthly by The Endocrine Society (http://www.endo-society.org), the foremost professional society serving the endocrine community.**